RESEARCH ARTICLE | OCTOBER 22 2025

# Direct detection of 14.1 MeV neutrons by multi-stacked h-BN detector $\odot$

G. Somasundaram <sup>(i)</sup>; Z. Alemoush <sup>(i)</sup>; J. Li <sup>(i)</sup>; J. Y. Lin <sup>(i)</sup>; H. X. Jiang <sup>(i)</sup>

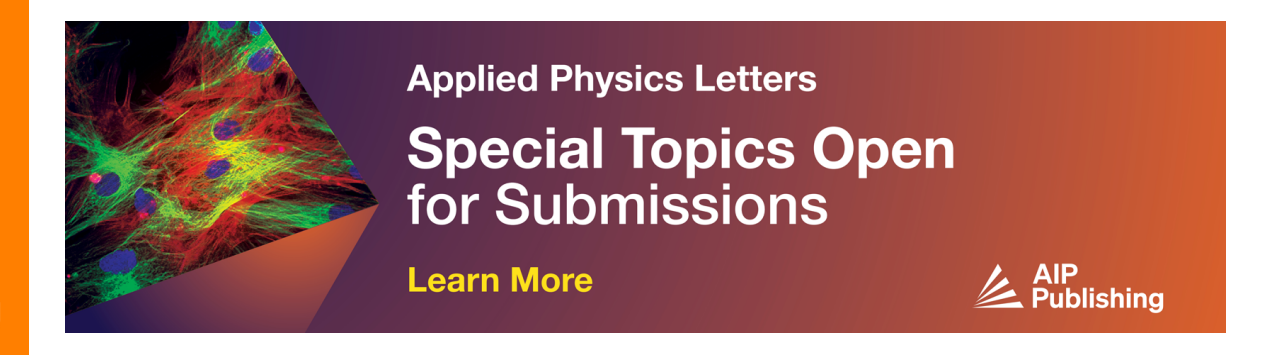


Appl. Phys. Lett. 127, 162103 (2025) https://doi.org/10.1063/5.0296469

A CHORUS









## Direct detection of 14.1 MeV neutrons by multi-stacked h-BN detector

Cite as: Appl. Phys. Lett. 127, 162103 (2025); doi: 10.1063/5.0296469 Submitted: 13 August 2025 · Accepted: 7 October 2025 · Published Online: 22 October 2025













## **AFFILIATIONS**

Department of Electrical and Computer Engineering, Texas Tech University, Lubbock, Texas 79409, USA

<sup>a)</sup>Author to whom correspondence should be addressed: hx.jiang@ttu.edu

## **ABSTRACT**

Reliable detection of 14.1 MeV neutrons from deuterium-tritium (DT) fusion reactions is vital for advancing nuclear energy, bolstering national security, and managing nuclear waste. Despite their importance, the effective detection of 14.1 MeV neutrons produced from these reactions remains a significant hurdle for semiconductor detectors, primarily due to their inherently low interaction cross section. We report here the development of a stacked detector constructed from hexagonal boron nitride (h-BN) quasi-bulk crystals produced by hydride vaporphase epitaxy (HVPE) growth. The mean free path ( $\lambda$ ) of 14.1 MeV fast neutrons in h-BN was determined to be 11.3 cm. By engineering an effective neutron interaction path length of 1 cm, we have achieved a notable neutron detection efficiency of 5.0% and a charge collection efficiency of 59% when exposed to 14.1 MeV fast neutrons. Furthermore, this stacked h-BN detector exhibits a substantial neutron-generated direct current, suggesting the feasibility for realizing portable and battery-powered DT neutron sensors. Our findings are a major step forward, with the potential to deliver highly sensitive, compact, scalable, and operationally efficient h-BN semiconductor fast neutron detectors that will benefit diverse scientific and industrial applications.

Published under an exclusive license by AIP Publishing. https://doi.org/10.1063/5.0296469

III-nitride wide-bandgap materials, such as GaN, AlN, and BN, have revolutionized various technologies, including solid-state lighting, visible and ultraviolet emitters and detectors, radio frequency (RF) communications, and high-temperature and high-power electronics. Among III-nitrides, hexagonal boron nitride (h-BN) stands out with an ultrawide bandgap (UWBG) of approximately  $6 \, \text{eV}$ ,  $^{14-16}$  a high breakdown electric field of  $\sim 12 \, \text{MV/cm}$ ,  $^{17}$  and outstanding in-plane thermal conductivity of ~550 W/m K. 18 Its layered crystalline structure also facilitates integration with other 2D and IIInitride materials, enabling advanced device architectures.11

Beyond traditional III-nitride applications, h-BN is an excellent material for solid-state neutron detectors by leveraging the <sup>10</sup>B(n,α)Li nuclear reaction for thermal neutron capture. 22,23 The theoretical detection efficiency  $(\eta_i)$  is directly related to detector thickness (d) by  $\eta_i = 1$  $-e^{-d/\lambda}$ , where  $\lambda$  is the thermal neutron absorption length (47  $\mu$ m for B-10 enriched h-BN and 237  $\mu$ m for natural h-BN). This relationship highlights the critical need for the development of thick h-BN epitaxial layers (or h-BN quasi-bulk crystals). Our group has made significant strides in this area, achieving a record-high thermal neutron detection efficiency of 60% by using 100 μm thick B-10 enriched h-BN epi-

On the other hand, detecting fast neutrons using compact semiconductor detectors is exceptionally difficult due to the extremely low interaction cross section of fast neutrons with matter, yet ideal. Despite this difficulty, fast neutron detectors are crucial for diverse applications, including nuclear security, reactor monitoring, space exploration, and advanced radiation-based medical treatments.<sup>28-</sup> particularly significant class is 14.1 MeV neutrons produced by the deuterium-tritium (DT) fusion reaction, which is central to fusion energy research and neutron source generation. The development of robust and efficient 14.1 MeV neutron detectors is critical for monitoring and controlling the fusion process, evaluating and mitigating the impact of neutron radiation on materials, and ensuring the efficient breeding of tritium fuel.<sup>33–36</sup> For compact microreactors designed for remote deployment, DT neutron generators provide a versatile and controllable neutron source. These generators support diagnostics, incore monitoring, and accelerated material testing, thereby contributing significantly to the development of next-generation compact nuclear technologies.3

Our previous work has demonstrated h-BN's ability to directly detect fast neutrons emitted from bare Cf-252 and AmBe neutron sources.  $^{32,37,38}$  We report here the growth of 1 mm thick h-BN quasi-bulk crystals by hydride vapor-phase epitaxy (HVPE) and the development of a stacked detector. By engineering an effective neutron interaction path length of 1 cm, we have achieved a notable neutron detection efficiency of 5.0% and a charge collection efficiency of 59%

for 14.1 MeV fast neutrons. Furthermore, a significant direct current (DC) response to 14.1 MeV fast neutrons has been measured, paving the way for direct analysis of radiation-induced current using compact and portable h-BN semiconductor detectors.

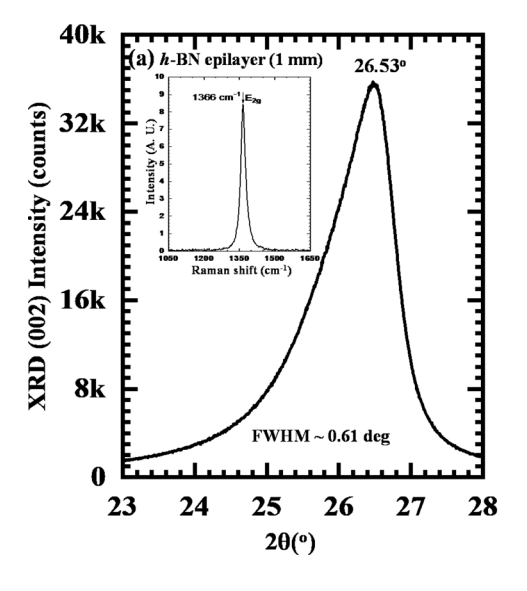
The 1 mm thick h-BN quasi-bulk wafers were grown on 4''diameter c-plane sapphires by HVPE, 26,27,32,38-41 which offers high growth rates and elimination of carbon impurities by using BCl3 as a precursor for boron and NH3 gas for nitrogen. The layered structure of h-BN enables a thick h-BN wafer to self-separate from the sapphire substrate during cooling down upon completion of growth, resulting in the formation of a freestanding h-BN wafer.  $^{24-27,32,38-41}$  Figure 1 shows an x-ray diffraction (XRD) spectrum in a  $2\theta$ - $\omega$  scan showing the diffraction peak corresponding to the (002) planes of h-BN, confirming that the 1 mm thick h-BN wafer retains a layered crystalline structure. However, the (002) reflection peak appeared at  $2\theta = 26.53^{\circ}$ , shifted to a smaller angle compared to  $2\theta = 26.72^{\circ}$  observed in 100  $\mu$ m thick freestanding h-BN wafers. 26,27,39 This shift suggests that the stacking sequence along the c-direction becomes less ordered with increasing thickness,<sup>38</sup> corroborating with our previous results which conclusively demonstrated that the electronic property assessed by carrier mobility-lifetime product enhances as layers of h-BN are successively removed from the top by polishing.<sup>38</sup> The full width at half maximum (FWHM) of the (002) peak of 1 mm thick wafer ( $\sim$ 1°) is also much broader than a value of  $0.29^{\circ}$  for  $100 \,\mu m$  thick freestanding wafers.2

The inset of Fig. 1(a) plots a Raman spectrum exhibiting a mode at  $\Delta \sigma = 1366 \, \mathrm{cm}^{-1}$ , corresponding to the  $E_{2g}$  vibration mode (in-plane stretch of B and N atoms), which again confirms a layered crystalline structure. However, the measured FWHM of about  $26 \, \mathrm{cm}^{-1}$  is much broader than the value of  $16 \, \mathrm{cm}^{-1}$  observed in our  $100 \, \mu \mathrm{m}$  thick freestanding wafers. <sup>39</sup> In h-BN, the inclusion of various polytype domains and structural disorders becomes more prevalent with increasing the layer thickness during h-BN growth because different stacking sequences have only a minor effect on the total energy of the layer-structured BN crystals. <sup>42</sup> There remains a need to explore growth and postgrowth processes to further improve the crystalline quality of h-BN wafers with a thickness exceeding 1 mm. <sup>43</sup>

The as-grown 1 mm-thick freestanding h-BN wafer was mechanically polished to a reduced thickness of 0.7 mm to improve surface smoothness. The wafer was subsequently diced into strips of 1.3 mm in width and 1 cm in length by laser dicing. Lateral detectors were fabricated by depositing metal contacts consisting of a bilayer of Ni (100 nm)/Au (40 nm) on the two edges of each h-BN strip via electronbeam evaporation.<sup>44</sup> Electrical characterization of the detector revealed a room temperature resistivity of  $8.1 \times 10^{13} \,\Omega$  cm, indicating excellent insulating properties. We first conducted photocurrent excitation spectroscopy (PES) measurement to assess the optoelectronic properties of this 1 mm thick freestanding wafer. The inset of Fig. 1(b) is an optical image of a fabricated device for PES measurements. A laser-driven light source (LDLS) covering a wavelength range between 190 and 2400 nm coupled with a triple grating monochromator was used as a variable wavelength excitation source. A photocurrent excitation spectrum measured at 100 V is shown in Fig. 1(b). Peaks in a photocurrent excitation spectrum represent direct photoexcitation of free carriers from either a band-to-band or impurity-to-band transition. The spectrum exhibits a dominant band edge transition peak around 6.2 eV, signifying that the 1 mm thick h-BN wafer produced by HVPE retains UWBG material properties. The spectrum also shows a weak peak at  $\sim$ 3.2 eV, indicating the presence of deep level impurities/defects.

By vertically stacking seven lateral detectors, a total detector thickness of 5 mm was achieved along the c-axis of h-BN. A highly resistive polyimide adhesive was used to mount the detector onto sapphire. Wire bonding was subsequently performed to electrically connect the detector strips in parallel through the bonding pads of a semiconductor device package. Figure 2(a) presents a schematic illustration of the vertically stacked seven-layer h-BN detector, while Figs. 2(b) and 2(c) show optical images of the assembled device. The 14.1 MeV neutrons with a beam size of approximately 1 cm in diameter were generated through the DT fusion reaction (Thermo Scientific P 385 DT neutron generator). The generator is operated in continuous mode, and the source effectively functioned as a point source due to the near-isotropic emission of neutrons.

To detect 14.1 MeV fast neutrons, the primary mechanism utilized is elastic scattering between the neutrons and the B and N atoms.



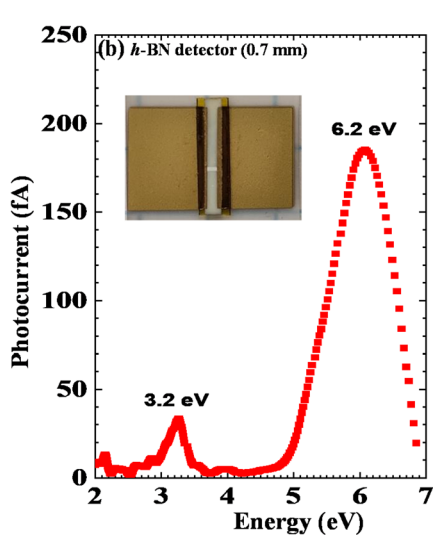


FIG. 1. Structural and optoelectronic properties of a 1 mm-thick freestanding h-BN wafer synthesized by HVPE. (a) X-ray diffraction (XRD) pattern in  $2\theta{-}\omega$  scan covering the (002) peak, and the inset is a Raman spectrum measured at 785 nm and (b) photocurrent excitation spectrum (PES), and the inset is a top view of a lateral detector used for the PES measurements, fabricated from the same 1 mm-thick freestanding h-BN wafer with an electrode spacing of 1.3 mm, a length of 1 cm, and a reduced thickness of 0.7 mm by mechanical polishing.

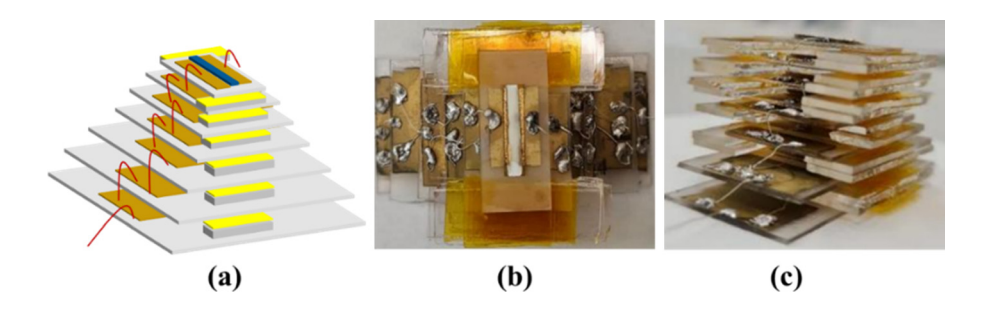


FIG. 2. (a) Schematic diagrams of the seven-layer stacked *h*-BN fast neutron detector, (b) top view, and (c) side view of the completed seven-layer stacked *h*-BN detector with a total thickness of 5 mm and dimensions of 1.3 mm (W) × 10 mm (L).

During elastic scattering, 14.1 MeV neutrons collide with a B or N atom, transferring a portion of their kinetic energy and creating a vacancy and an interstitial defect. The recoiling nuclei, energized by this collision, traverse the detector medium and lose energy primarily through ionization, resulting in the generation of electron–hole pairs. The subsequent collection of these charge carriers under an applied electric field serves as the measurable signal for fast neutron detection. The recoil energy  $(E_R)$  of a B or N atom is described by the following equation:  $^{33,37}$ 

$$E_R = [4A/(1+A)^2](\cos^2\theta_s)E_N,$$
 (1)

where A is the atomic number, and A = 10, 11, and 14 for B-10 (20%), B-11 (80%), and N-14 (100%) in natural BN,  $\theta$  represents the recoiling angle of the recoiling element, and  $E_N$  represents the neutron energy (14.1 MeV). The number of electron–hole pairs generated, denoted as  $N_e = N_h$ , can be estimated by assuming that approximately  $3E_g$  is required to generate one electron–hole pair, where  $E_g$  is the bandgap energy of h-BN.  $^{46,47}$  Thus, the number of pairs can be expressed as  $N_e = N_h = E_R/3E_g$ . According to Eq. (1), the recoil energy  $(E_R)$  imparted to a target nucleus increases as the atomic number A of the scattering element decreases. B and N possess some of the lowest atomic numbers among the constituents of inorganic semiconductors, offering a significant advantage. At a given neutron energy  $(E_N)$ , fast neutrons can transfer a greater fraction of their energy to these light nuclei, resulting in higher recoil energies  $(E_R)$ . This, in turn, generates a larger number of free charge carriers within the BN crystal, thereby enhancing the

overall detection efficiency. The elastic scattering results in an average recoiling energy of  $E_R \sim 1.38$  MeV in BN based on Eq. (1).

We first attempted to determine the mean free path of 14.1 MeV fast neutrons in h-BN, which is necessary for the evaluation of theoretical detection efficiency for a given detector thickness. To do this, we measured neutron transmission through pyrolytic BN (p-BN) films of different thicknesses, as we have done for Cf-252 and AmBe neutron sources. Although p-BN does not support the collection of neutron-induced charge carriers, its crystal structural properties are like h-BN. As a result, the transmission behavior of 14.1 MeV fast neutrons in p-BN serves as a reliable approximation for that in h-BN crystals.

Figure 3(a) shows the experimental setup used to measure the transmission of 14.1 MeV fast neutrons in p-BN. In this setup, we measured the relative transmission (T) of 14.1 MeV fast neutrons through p-BN films with varying thicknesses (d) by recording neutron counts received by the stacked h-BN detector. Figure 3(b) illustrates the arrangement of the stacked h-BN neutron detector and its position relative to the 14.1 MeV DT neutron source. In Fig. 3(c), the measured transmission data are shown as solid squares, indicating the relative neutron flux successfully passing through p-BN films of different thicknesses. The measured transmission (T) of 14.1 MeV neutrons through p-BN can be expressed using the standard absorption/transmission equation

$$T = \exp\left(-\frac{d}{\lambda}\right),\tag{2}$$

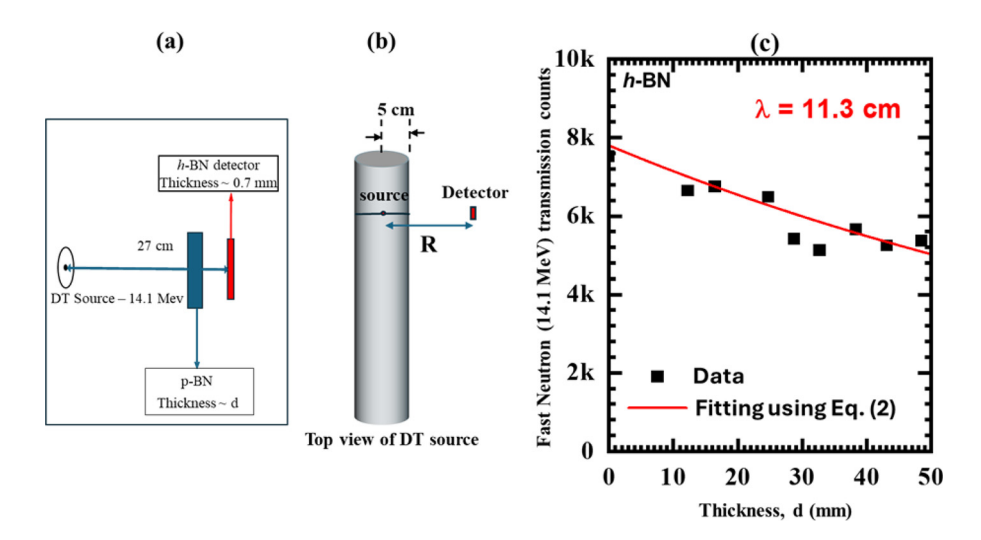


FIG. 3. (a) Schematic of the experimental setup for neutron transmission measurements using a 14.1 MeV DT source. Pyrolytic BN (p-BN) films were used in lieu of h-BN, and the relative neutron flux passing through pyrolytic BN films of varying thicknesses (d) was recorded, (b) top view of the 14.1 MeV DT source showing the position of the stacked fast neutron detector, and (c) measured 14.1 MeV neutron transmission (T) as a function of BN layer thickness. The solid red curve represents the least squares fit of the data to Eq. (2).

where d is the neutron interaction path length, and  $\lambda$  is the mean free path of 14.1 MeV fast neutrons in h-BN. The measured data (solid squares) can be fitted very well using Eq. (2), yielding a mean free path ( $\lambda$ ) of 11.3 cm for 14.1 MeV fast neutrons in h-BN, as shown by the red curve in Fig. 3(c).

To further validate the measurement result, we can also estimate the mean free path of 14.1 MeV neutrons in h-BN. The elastic scattering cross sections of 14.1 MeV neutrons with B-10, B-11, and N-14 are 0.908, 0.794, and 0.969 barns, respectively. Natural h-BN comprises 20% of B-10 and 80% of B-11, and the atomic densities of B-10, B-11, and N-14 atoms in natural h-BN are  $1.1 \times 10^{22}$ ,  $4.4 \times 10^{22}$ , and  $5.5 \times 10^{22}$  atoms/cm³, respectively. The macroscopic elastic scattering cross section ( $\Sigma$ ) can be calculated to be [ $\Sigma = N\sigma = \{[(0.908) \times (1.1 \times 10^{22})] + [(0.794) \times (4.4 \times 10^{22})] + [(0.969) \times (5.5 \times 10^{22})] \times 10^{-24}$  cm<sup>-1</sup>} = 0.09 cm<sup>-1</sup>], providing the theoretical mean free path length of 14.1 MeV neutrons in h-BN to be  $\lambda = \Sigma^{-1} = (0.09 \text{ cm}^{-1})^{-1} = 11.1 \text{ cm}$ , which is in excellent agreement with the experimentally measured data of 11.3 cm for 14.1 MeV neutrons.

By knowing  $\lambda$ , the intrinsic detection efficiency of h-BN detector can be evaluated according to the interaction probability and is written as

$$\eta_i = 1 - T = 1 - \exp\left(-\frac{d}{\lambda}\right). \tag{3}$$

Based on this relationship, achieving an intrinsic detection efficiency greater than 63% (where  $d=\lambda$ ) for 14.1 MeV neutrons would require an h-BN detector incorporating a neutron interaction path length of d>11.3 cm. In the case of the seven-layer stacked h-BN neutron detector with a total thickness of 5 mm used in this study, the expected intrinsic detection efficiency for 14.1 MeV fast neutrons is  $(1-\exp(-0.5/11.3))=4.3\%$  if the oncoming neutrons' path is parallel to the c-axis. The analysis highlights both the potential and the limitations of the stacked h-BN detector designs for the direct detection of 14.1 MeV neutrons, as well as the need for further scaling the wafer thickness to achieve higher efficiency.

To evaluate the detection efficiency, the detector was operated in a particle counting mode utilizing pulse height spectrum (PHS) analysis, following the methodology previously established for h-BN neutron detectors. 49,50 Since h-BN neutron detectors are highly sensitive to thermal neutrons, a 2.1 mm-thick (p-BN) film was placed in front of the DT source as a thermal neutron shield to eliminate thermal neutron interference. For PHS measurements, deuterons were accelerated to 90 kV and directed onto a tritiated titanium target, with a beam current of 50  $\mu$ A, providing a neutron emission rate of  $1.0 \times 10^8$  n/s. The stacked h-BN detector was positioned 27 cm away from the neutron source, corresponding to a neutron flux on the detector surface of  $1.1 \times 10^4$  n/s cm<sup>2</sup>, as illustrated in Fig. 3(b). Since the cross section of this stacked detector is sufficiently large ( $5 \times 1.3$  mm), we carried out efficiency measurements in two configurations to assess the crystal orientation dependence of the charge collection efficiency: (a) the neutron beam is aligned parallel to the c-axis, as illustrated in the inset (a) of Fig. 4; and (b) the neutron beam is aligned parallel to the c-plane, as illustrated in the inset (b) of Fig. 4. The configuration shown in the inset (b) of Fig. 4 utilizes a longer neutron interaction path length of 1 cm along the c-plane than that along the c-axis (which is the total thickness of the stacked detector of 5 mm).

Figure 4 plots the measured PHS of the h-BN fast neutron detector in response to 14.1 MeV DT neutrons when the neutron beam is

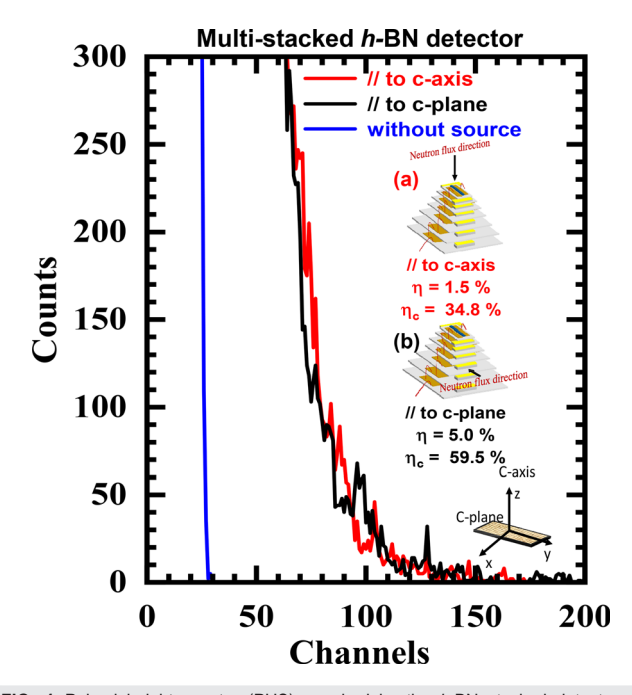


**FIG. 4.** Pulsed height spectra (PHS) acquired by the *h*-BN stacked detector of 5 mm in thickness and 1 cm in length in response to 14.1 MeV fast neutrons parallel to the c-axis (red curve), parallel to the c-plane (black curve), and in the absence of any source (blue curve). Measurements were conducted at a bias voltage of 450 V and a detector at 27 cm from the 14.1 MeV DT source with a neutron emission rate of  $1.0 \times 10^8$  n/s, resulting in a neutron flux of  $1.1 \times 10^4$  n/s cm² on the detector. A 2.1 mm thick p-BN layer was used to block thermal neutrons from the neutron source. The insets illustrate the neutron beam directions: (a) parallel to the c-axis and (b) parallel to the c-plane.

aligned parallel to the c-axis (red curve) and the c-plane (black curve), along with the background response in the absence of neutron exposure (blue curve). When the neutron beam is aligned parallel to the cplane, it traverses across the layered structure of h-BN, resulting in a longer interaction path of 1 cm within the detector and thereby increasing the probability of neutron interaction. In contrast, alignment parallel to the c-axis directs the neutron beam along the stacking direction of the h-BN layers with a neutron interaction path length of 0.5 cm. By rotating the detector, the effective neutron path length can be controlled without altering the detector's physical thickness. This configuration enables evaluation of the directional dependence of detection efficiency and provides insight into real-world performance under varying irradiation geometries. The measurements were performed at a bias voltage of 450 V. Notably, the h-BN detector demonstrates negligible sensitivity to gamma radiation, 24-27,32,37,3 ensuring a clean neutron signal.

When the neutron beam was aligned parallel to the c-plane (10 mm neutron path length), over a 15 min measurement time period, the neutron counts acquired by the detector were 32 399, corresponding to a flux of  $\frac{32\,399}{15\times60\times(0.13\times0.5)}=553$  n/s cm² and a detection efficiency ( $\eta)=\frac{553}{1.1\times10^4}=5.0\%$ . In comparison, the neutron counts registered by the detector were 19 806 over a 15 min count time, corresponding to a flux of  $\frac{19\,806}{15\times60\times(0.13\times1.0)}=170$  n/s cm² and a detection efficiency ( $\eta)=\frac{170}{11\times10^4}=1.5\%$ , when the neutron beam is aligned parallel to the

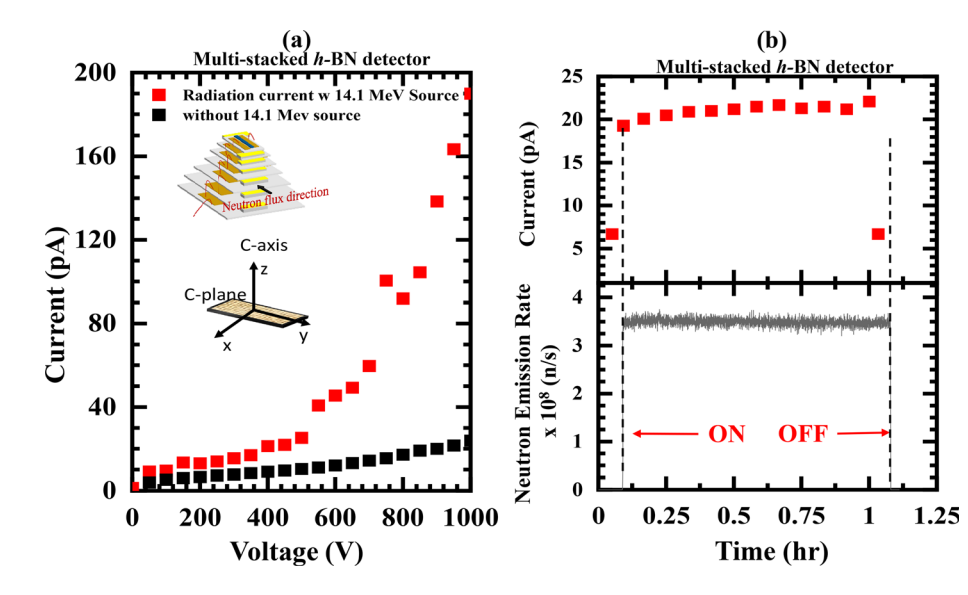


**FIG. 5.** (a) DC response of a stacked h-BN detector with a total thickness of 5 mm and dimensions of 1.3 mm (W)  $\times$  10 mm (L) in response to 14.1 MeV fast neutrons, with neutron flux incident along the c-plane. The detector was placed at 5 cm from the neutron source with a neutron emission rate set at  $3.4 \times 10^8$  n/s. (b) The DT neutron-generated DC response as a function of the irradiation time at a bias voltage of 450 V.

c-axis (5 mm neutron path length). Based on Eq. (3), the intrinsic detection efficiencies of 8.4% and 4.3% are derived using 11.3 cm as the mean free path. By defining the charge collection efficiency as the ratio of the measured efficiency to the intrinsic efficiency, the corresponding charge collection efficiencies are 59.5% and 34.8% for neutron propagation along the c-plane and the c-axis, respectively. The results suggest that the detection efficiency enhancement in the direction parallel to the c-plane is not only attributed to an enhanced elastic scattering interaction probability facilitated by the increased neutron path length or material volume but also an enhanced charge collection efficiency, a result most likely related to the layered crystalline structure of h-BN. The results suggest that utilizing the neutron path parallel to the c-plane is advantageous over that parallel to the c-axis. More importantly, in terms of device processing, it is easier to increase the path length along the c-plane, which is limited by the wafer size, whereas the neutron path length along the c-axis is currently limited by our ability of producing thick *h*-BN wafers. It is worth noting that elastic scattering between fast neutrons and B and N atoms will not create a sufficient defect density, which otherwise would affect the performance of BN neutron detectors.

Additionally, we have investigated the detector's ability to operate in a direct current (DC) mode under continuous irradiation to evaluate its real-time operational behavior. DCs were measured using the configuration of the neutron beam directed along the c-plane to utilize the 1.0 cm neutron path length, as schematically shown in the inset of Fig. 5(a). To obtain a more prominent DC signal, we increased the DT neutron emission rate to  $3.4 \times 10^8$  n/s by accelerating deuterons to 130 kV and simultaneously decreased the distance between the source and detector to 5 cm, providing an incident neutron flux of  $1.1 \times 10^6$  n/s cm<sup>2</sup> on the detector's cross section. The main plot displays the radiationinduced current as a function of applied bias voltage, demonstrating a nearly linear dependence below 500 V and a nonlinear increase in current with increasing bias voltage above 500 V. The transition from linear to nonlinear I-V characteristics may be accounted for by the effect of electric field-induced lowering of a

potential energy barrier at a metal–semiconductor interface or trapping sites. The properties of contacts on highly resistive UWBG materials represent another very important research topic for further investigation and understanding.<sup>41</sup>

Figure 5(b) provides additional insight into the detector's DC response characteristics under controlled neutron irradiation. For the experimental data shown in Fig. 5(b), the DC is monitored by an electrometer (Keithley 617) with a slow response time (1 s). The lower panel shows an on/off switching behavior of the DT neutron source. The upper panel plots the radiation-induced current in response to modulated neutron exposure, confirming that the current is indeed neutron-induced rather than arising from background noise or thermal drift. At a fixed bias voltage, the magnitude of neutron-generated current is nearly constant with irradiation time.

The demonstrated capability of DC operation mode provides several advantages. For instance, DC mode allows for the collection of real-time data without the need for gating or timing circuits as those required for acquiring the pulsed height spectra shown in Fig. 4, facilitating immediate analysis and response, and is ideal for applications where real-time data are crucial. The output from DC mode is typically a steady signal proportional to the neutron count rate, which can simplify data processing and analysis compared to the more complex signal processing required in pulse mode. DC detection systems have simpler electronic requirements and may consume less power compared to pulse mode detectors, making them more suitable for portable or battery-operated applications.

In summary, we have fabricated a multi-stacked h-BN neutron detector from quasi-bulk h-BN wafers grown via HVPE. We determined the mean free path of 14.1 MeV fast neutrons in h-BN to be 11.3 cm and demonstrated the direct detection of 14.1 MeV fast neutrons with a detection efficiency of up to 5.0%. Continuous-wave (CW) measurements validated a clear and reproducible DC response to modulated neutron flux. The present and previous results position h-BN quasi-bulk crystals as a highly promising candidate for future solid-state detectors for both thermal and fast neutrons, offering

significant advantages in scalability, stability, and operational efficiency. Continued innovation in h-BN crystal quality and advancements in thickness scalability are essential steps to further enhance detection efficiency and unlock the widespread deployment of these detectors in critical scientific, industrial, and nuclear security applications.

The information, data, or work presented herein was funded in part by the Advanced Research Projects Agency-Energy (ARPA-E), U.S. Department of Energy, under Award No. DE-AR0001552 monitored by Dr. Olga Spahn and Dr. Eric Carlson. The views and opinions of authors expressed herein do not necessarily state or reflect those of the United States Government or any agency thereof. Jiang and Lin are grateful to the AT&T Foundation for the support of Ed Whitacre and Linda Whitacre endowed chairs. The authors gratefully acknowledge Ian Django Jones from the Department of Physics at Texas Tech University for his assistance in operating the 14.1 MeV DT neutron source.

## AUTHOR DECLARATIONS

### **Conflict of Interest**

The authors have no conflicts to disclose.

## **Author Contributions**

Gokul Somasundaram: Data curation (equal); Formal analysis (equal); Investigation (equal); Methodology (equal); Software (equal); Validation (equal); Visualization (equal); Writing - original draft (equal). Zaid Alemoush: Data curation (equal); Formal analysis (equal); Investigation (equal); Methodology (equal); Software (equal); Validation (equal); Visualization (equal). Jing Li: Data curation (equal); Formal analysis (equal); Investigation (equal); Methodology (equal); Project administration (equal); Resources (equal); Software (equal); Supervision (equal); Validation (equal); Visualization (equal). Jingyu Lin: Conceptualization (equal); Formal analysis (equal); Funding acquisition (equal); Investigation (equal); Methodology (equal); Project administration (equal); Resources (equal); Supervision (equal); Validation (equal); Visualization (equal); Writing - review & editing (equal). Hongxing Jiang: Conceptualization (equal); Formal analysis (equal); Funding acquisition (equal); Investigation (equal); Methodology (equal); Project administration (equal); Resources (equal); Supervision (equal); Validation (equal); Visualization (equal); Writing - original draft (equal); Writing - review & editing (equal).

## DATA AVAILABILITY

The data that support the findings of this study are available within the article.

## **REFERENCES**

- <sup>1</sup>See https://www.nobelprize.org/prizes/physics/2014/press-release/ for "The Nobel prize in physics" (2014).
- <sup>2</sup>H. Amano, N. Sawaki, I. Akasaki, and Y. Toyoda, Appl. Phys. Lett. 48, 353 (1986).
- <sup>3</sup>S. Nakamura, T. Mukai, and M. Senoh, Appl. Phys. Lett. **64**, 1687 (1994).
- <sup>4</sup>T. D. Moustakas, U.S. patent 5,686,738 (1997).
- <sup>5</sup>M. A. Khan, K. Balakrishnan, and T. Katona, Nat. Photonics 2, 77 (2008).
- <sup>6</sup>S. Pimputkar, J. S. Speck, S. P. DenBaars, and S. Nakamura, Nat. Photonics 3, 180 (2009)

- <sup>7</sup>M. E. Levinshtein, S. L. Rumyantsev, and M. S. Shur, *Properties of Advanced Semiconductor Materials: GaN, AlN, InN, BN, SiC, SiGe*, edited by M. E. Levinshtein, S. L. Rumyantsev, and M. S. Shur (John Wiley & Sons, 2001).
- <sup>8</sup>H. X. Jiang and J. Y. Lin, Nat. Electron. **6**, 257 (2023).
- <sup>9</sup>P. J. Parbrook, B. Corbett, J. Han, T. Y. Seong, and H. Amano, Laser Photonics Rev. 15, 2000133 (2021).
- <sup>10</sup>M. A. Khan, A. Bhattarai, J. N. Kuznia, and D. T. Olson, Appl. Phys. Lett. 63, 1214 (1993).
- <sup>11</sup>Y. H. Chen, J. Encomendero, C. Savant, V. Protasenko, H. G. Xing, and D. Jena, Appl. Phys. Lett. **124**, 152111 (2024).
- H. Amano, Y. Baines, E. Beam *et al.*, J. Phys. D: Appl. Phys. 51, 163001 (2018).
   M. Higashiwaki, R. Kaplar, J. Pernot, and H. Zhao, Appl. Phys. Lett. 118, 200401 (2021).
- <sup>14</sup>T. Sugino, K. Tanioka, S. Kawasaki, and J. Shirafuji, Jpn. J. Appl. Phys. 36, L463 (1997).
- <sup>15</sup>B. Arnaud, S. Lebe'gue, P. Rabiller, and M. Alouani, Phys. Rev. Lett. **96**, 026402 (2006).
- 16 G. Cassabois, P. Valvin, and B. Gil, Nat. Photonics 10, 262 (2016).
- <sup>17</sup>Y. Hattori, T. Taniguchi, K. Watanabe, and K. Nagashio, Appl. Phys. Lett. 109, 253111 (2016).
- <sup>18</sup>C. Yuan, J. Li, L. Lindsay, D. Cherns, J. W. Pomeroy, S. Liu, J. H. Edgar, and M. Kuball, Commun. Phys. 2, 43 (2019).
- <sup>19</sup>A. K. Geim and I. V. Grigorieva, "Van der Waals heterostructures," Nature 499, 419 (2013).
- 20 Y. Wu, Y. Xiao, Y. Zhao, and Z. Mi, Proc. Natl. Acad. Sci. 122, e2417859122 (2025)
- <sup>21</sup>Y. Gao, X. Lin, T. Smart, P. Ci, K. Watanabe, T. Taniguchi, R. Jeanloz, J. Ni, and J. Wu, Phys. Rev. Lett. 125, 226403 (2020).
- <sup>22</sup>O. Osberghaus, Z. Phys. **128**, 366 (1950).
- <sup>23</sup>G. F. Knoll, Radiation Detection and Measurement, 4th ed. (John Wiley & Sons, Hoboken, NJ, 2010).
- <sup>24</sup>A. Maity, S. J. Grenadier, J. Li, J. Y. Lin, and H. X. Jiang, Prog. Quantum. Electron 76, 100302 (2021).
- <sup>25</sup>A. Maity, S. J. Grenadier, J. Li, J. Y. Lin, and H. X. Jiang, Appl. Phys. Lett. 116, 142102 (2020).
- <sup>26</sup>H. X. Jiang and J. Y. Lin, Phys. Status Solidi B **2025**, 2400605.
- <sup>27</sup>Z. Alemoush, A. Tingsuwatit, A. Maity, J. Li, J. Y. Lin, and H. X. Jiang, J. Appl. Phys. 135, 175704 (2024).
- <sup>28</sup>R. C. Runkle, Nucl. Instrum. Methods Phys. Res., Sect. A **652**, 37 (2011).
- <sup>29</sup>U. Wo'Znicka, J. Fusion Energy **38**, 376 (2019).
- <sup>30</sup>G. Ericsson, J. Fusion Energy **38**, 330 (2019).
- 31B. M. van der Ende, L. Li, D. Godin, and B. Sur, Nat. Commun. 10, 1959 (2019).
- <sup>32</sup>J. Li, A. Tingsuwatit, Z. Alemoush, J. Y. Lin, and H. X. Jiang, APL Mater. 13, 011101 (2025).
- <sup>53</sup>I. Radia, IAEA Radiation Technology Reports No. 1, ISSN 2225-8833 (2012). https://www.pub.iaea.org/MTCD/Publications/PDF/P1535\_web.pdf
- <sup>34</sup>T. Stainer, M. R. Gilbert, L. W. Packer, S. Lilley, V. Gopakumar, and C. Wilson, EPJ Web Conf. 247, 09010 (2021).
- 35J. F. Stubbins, "Review of advanced manufacturing technologies for fusion reactor materials," Technical Report (Office of Nuclear Regulatory Research, U.S. Nuclear Regulatory Commission, 2024), https://www.nrc.gov/docs/ML2413/
- ML24137A055.pdf.
  <sup>36</sup>J. Jeet, A. B. Zylstra, M. Rubery, Y. Kim, K. D. Meaney, C. Forrest, V. Glebov, C. J. Horsfield, A. M. McEvoy, and H. W. Herrmann, Phys. Rev. C 104, 054611
- <sup>37</sup>A. Tingsuwatit, A. Maity, S. J. Grenadier, J. Li, J. Y. Lin, and H. X. Jiang, Appl. Phys. Lett. **120**, 232103 (2022).
- <sup>38</sup>G. Somasundaram, N. K. Hossain, Z. Alemoush, A. Tingsuwatit, J. Li, J. Y. Lin, and H. X. Jiang, Appl. Phys. Lett. **126**, 212104 (2025).
- <sup>39</sup>N. K. Hossain, A. Tingsuwatit, Z. Alemoush, M. Almohammad, J. Li, J. Y. Lin, and H. X. Jiang, Appl. Phys. Express 17, 091001 (2024).
- 40 Z. Alemoush, A. Tingsuwatit, J. Li, J. Y. Lin, and H. X. Jiang, Crystals 13, 1319
- <sup>41</sup>A. Tingsuwatit, N. K. Hossain, Z. Alemoush, M. Almohammad, J. Li, J. Y. Lin, and H. X. Jiang, Appl. Phys. Lett. 124, 162105 (2024).
- <sup>42</sup>K. A. Mengle and E. Kioupakis, APL Mater. 7, 021106 (2019).

- N. K. Hossain, G. Somasundaram, Z. Alemoush, J. Li, J. Y. Lin, and H. X. Jiang, Appl. Phys. Lett. 126, 202107 (2025).
   A. Maity, S. J. Grenadier, J. Li, J. Y. Lin, and H. X. Jiang, Appl. Phys. 123,
- 044501 (2018).
- 45 P. Kerr, C. Nerine, C. Jennifer, G. Gary, H. Jim, M. Colby, and O. N. Sean, Radiat. Detect. Technol. Methods 6, 234 (2022).
- <sup>46</sup>C. A. Klein, J. Appl. Phys. **39**, 2029 (1968).

- <sup>47</sup>R. C. Alig and S. Bloom, Phys. Rev. Lett. 35, 1522 (1975).
   <sup>48</sup>M. Baba, M. Ono, N. Yabuta, T. Kikuti, and N. Hirakawa, Radiat. Eff. 92, 223
- (1986).

  49S. J. Grenadier, "Advancements in hexagonal boron nitride for thermal neutron detection applications," Ph.D. thesis (Texas Tech University, 2020).
- 50 A. Maity, "Highly sensitive hexagonal boron nitride thermal neutron detectors," Ph.D. thesis (Texas Tech University, 2020).